Journal of Computational Physics 228 (2009) 938–951

Contents lists available at ScienceDirect

Journal of Computational Physics

journal homepage: www.elsevier.com/locate/jcp

Shape optimization towards stability in constrained hydrodynamic systems

Vincent Heuveline *, Frank Strauß

Computing Center and Institute for Applied and Numerical Mathematics, University of Karlsruhe, D-76128 Karlsruhe, Germany

ARTICLE INFO

Article history:
Received 27 November 2007
Received in revised form 17 June 2008
Accepted 18 June 2008
Available online 15 July 2008

Keywords:
Shape optimization
Hydrodynamic stability
Navier–Stokes equations
Eigenvalue problem

ABSTRACT

Hydrodynamic stability plays a crucial role for many applications. Existing approaches focus on the dependence of the stability properties on control parameters such as the Reynolds or the Rayleigh number. In this paper we propose a numerical method which aims at solving shape optimization problems in the context of hydrodynamic stability. The considered approach allows to guarantee hydrodynamic stability by modifying parts of the underlying geometry within a certain flow regime. This leads to a formulation of a shape optimization problem with constraints on the eigenvalues related to the linearized Navier–Stokes equations. In that context the eigenvalue problem is generally non-symmetric and may involve complex eigenvalues. To validate the proposed numerical approach we consider the flow around a body in a channel. The shape of the body is parameterized and can be changed by means of a discrete number of design variables. It is our aim to find a design which minimizes the drag force and ensures at the same time hydrodynamic stability while keeping the volume of the body constant. The numerical results show that a transition from an unstable design to a stable one is attainable by considering an adequate change of the body shape. The resulting bodies are long and flat which corresponds to common intuition.

1. Introduction

Hydrodynamic stability plays a crucial role for many applications where fluid flows are unstable in the sense that small perturbations superimposed on the mean flow can amplify and significantly disturb the basic state. With respect to the concept of stability several approaches have been devised which provide rigorous results but allow to depict only some facets of the highly complex physical mechanism leading to instability. The energy method ensures for example exponential decay in time of the energy of the system as well as unconditional stability assuming that some control parameters are below a critical value (see, e.g. [1] and references therein). An unconditional stability means that this property does not depend on the size of the initial perturbation. In many systems the information provided by the energy method is however quite pessimistic and the stability region which is provided is far away from the experimentally observed onset of instabilities (see [2]). Methods based on generalized energy functionals intend to cope with this issue and lead to conditional stability statements [3,4]. The method of linearized stability provides statements on conditional stability on the basis of a non-symmetric eigenvalue problem related to the linearized operator of the Navier–Stokes equation (see, e.g. [5]).

All these approaches have in common that they analyze the dependence between the stability properties and the value of a control parameter, usually the Reynolds number *Re* in a purely hydrodynamic system or the Rayleigh number *Ra* in Bénard convection. In that context prototypical systems are for example the Couette and the Poiseuille flow, the Rayleigh–Bénard and the Taylor–Couette system. A comprehensive overview is given in [2,6].

* Corresponding author.
E-mail address: vincent.heuveline@kit.edu (V. Heuveline).

0021-9991/$ - see front matter © 2008 Elsevier Inc. All rights reserved.
doi:10.1016/j.jcp.2008.06.030

In this paper we enlarge the class of such problems of stability to the case of shape optimization problems. We focus on a numerical approach which allows to determine optimal shape in the context of flow problems in that it minimizes a given cost functional while satisfying stability constraints with respect to the underlying flow. Since two decades shape optimization in fluids and flow control is a major research topic (see [7–11,15] and references therein). To the knowledge of the authors this type of problems has not been addressed so far in the context of stability by means of numerical methods despite their high relevance in many applications. This is mainly due to the fact that both topics, shape optimization and hydrodynamic stability, are generally highly challenging numerical problems on their own considering complex flow configurations.

To illustrate and validate numerically the proposed approach we consider the configuration of a flow in channel around a body whose shape is optimized towards the minimization of the acting drag forces. The underlying configuration is depicted in Fig. 4. For the case of a disk, benchmark computations with a main emphasis on the efficiency of the underlying numerical solver are summarized in [12]. Stability results for this type of problems can be found in [13,14]. In our approach the shape of the body inside the channel is parameterized. The corresponding parameters play the role of the design variables in the shape optimization problem. It is our aim to find a design which minimizes the drag forces and ensures linear stability of the hydrodynamic system.

The further contents of this paper are as follows: In Section 2 we discuss the special features of the considered shape optimization problem particularly the formulation of the linear stability constraints for the incompressible Navier–Stokes equations in that context. Section 3 introduces the details of the parameterization of the body inside the channel by means of quadratic as well as cubic spline approximations. Then, Section 4 outlines the proposed numerical method to solve this type of problems. The main emphasis is given to the development of a multigrid based Davidson method for the eigenvalue computation as well as an adequate SQP algorithm in that context. Numerical results for a benchmark flow problem are presented in Section 5. Finally, Section 6 is dedicated to the conclusions and we point out possible outcomes and future research topics related to the presented approach.

2. Linear stability and problem formulation

In a bounded domain $\Omega_q \subset \mathbb{R}^d$, where $d = 2$ or $d = 3$, we consider a base flow $\hat{u} := \{\hat{v}, \hat{p}\}$, determined by the stationary Navier–Stokes equations describing viscous, incompressible Newtonian fluid flow,

$$\begin{aligned} &-\nu\Delta\hat{v} + \hat{v}\cdot\nabla\hat{v} + \nabla\hat{p} = f \quad \text{in } \Omega_q,\\ &\nabla\cdot\hat{v} = 0 \quad \text{in } \Omega_q, \end{aligned} \tag{1}$$

where $\hat{v}$ describes the velocity vector field, $\hat{p}$ denotes the pressure, ν is the kinematic viscosity and f is a prescribed volume force. For ease of presentation we assume here that the density $\rho \equiv 1$. The subscript q in the notation Ω_q describes the parameterization of the underlying computational domain. We assume q to be a finite-dimensional vector. Furthermore, problem (1) is assumed to have a unique solution and that for a solution operator S the relation $\hat{u} = S(q)$ holds. At the boundary $\partial\Omega_q$, the usual non-slip boundary conditions are imposed along rigid parts together with suitable inflow and free-stream outflow conditions,

$$\hat{v}|_{\Gamma_{\text{rigid}}} = 0, \quad \hat{v}|_{\Gamma_{\text{in}}} = \hat{v}_{\text{in}}, \quad \nu\partial_n\hat{v} - \hat{p}n|_{\Gamma_{\text{out}}} = 0. \tag{2}$$

In our framework we consider the hydrodynamic stability by means of linear stability. This method relies on the solution of the eigenvalue problem related to the linearization of (1) about $\hat{u}$.

$$\begin{aligned} &A(\hat{u})(u) = -\nu\Delta v + \hat{v}\cdot\nabla v + v\cdot\nabla\hat{v} + \nabla p = \lambda v \quad \text{in } \Omega_q,\\ &\nabla\cdot v = 0 \quad \text{in } \Omega_q, \end{aligned} \tag{3}$$

for nonzero $u := \{v,p\} \in V$ and $\lambda \in \mathbb{C}$, under homogeneous boundary conditions (2). Here, $V \subset H^1(\Omega_q)^d \times L^2(\Omega_q)$ is a suitable subspace according to the prescribed boundary conditions (2). Obviously, this eigenvalue problem is non-symmetric and may possess complex eigenvalues. If an eigenvalue of (3) has $Re\lambda < 0$, then the base solution $\hat{u}$ is unstable, otherwise it is said to be linearly stable (see, e.g. [2]).

The shape of the geometry is described by a spline function representation. Certain parameters of this representation are taken as design variables. It is important to note that the proposed method can be used in a very general setup both with respect to the body description as well as the goal functional. Within this context the shape optimization problem we want to solve is formulated as follows:

$$\begin{aligned} &\min_q J(q) = F_D(q)\\ &\text{s.t.}\\ &Re(\lambda_{\min}(A(S(q)))) \geqslant 0,\\ &\underline{q} \leqslant q \leqslant \bar{q}, \end{aligned} \tag{4}$$

where q is a design variable vector consisting of parameters for the description of the body by spline functions. The vectors $\underline{q}$ and $\bar{q}$ are lower and upper bounds for the parameters due to restrictions on the geometry of the body. The drag force acting on the body B is given by (cf. Fig. 4)

$$F_D = \int_B \left(\rho \nu \frac{\partial u_t}{\partial n} n_y - p n_x \right) dS,$$

where ∂S is the surface of the object, n is the normal vector on S with its components n_x, n_y. The tangential velocity on S is denoted by u_t and the tangent vector is defined by $(n_y, -n_x)$. During the design process it turns out that additional constraints on the body B, e.g. volume restriction, are physically meaningful. They lead to the following optimization problem:

$$\begin{aligned} &\min_q J(q) = F_D(q) \\ &\text{s.t.} \\ &Re(\lambda_{\min}(A(S(q)))) \geqslant 0, \\ &\mathrm{vol}(B) = \mathrm{const}, \\ &\underline{q} \leqslant q \leqslant \bar{q}. \end{aligned} \tag{5}$$

3. Shape parameterization

For the description of the shape of the body we use approximations by spline functions consisting of compositions of quadratic as well as cubic Bézier curves (see, e.g. [16]). We focus on the description in just one quadrant using symmetry properties for the other parts.

3.1. Approximation by quadratic spline functions

A parametric quadratic Bézier curve $b : [0,1] \to \mathbb{R}^2$ is defined as linear combination

$$b(t) = \sum_{j=0}^{2} b_j B_j^{(2)}(t)$$

with given control points $b_0, b_1, b_2 \in \mathbb{R}^2$, where $b_j = (b_{j,x}, b_{j,y})$, and Bernstein polynomials

$$B_j^{(2)}(t) = \binom{2}{j} t^j (1-t)^{2-j}, \quad t \in [0,1].$$

We assume a symmetric body whose center is the origin of a suitably selected coordinate system. In each quadrant we construct a spline function consisting of two quadratic Bézier curves. We have for $i = 0, 1$

$$b(t) = \sum_{j=0}^{2} b_{2i+j} B_j^2 \left(\frac{t - t_i}{t_{i+1} - t_i} \right) \quad \text{on} \quad t \in [t_i, t_{i+1}],$$

where $0 = t_0 < t_1 < t_2 = 1$. As fixed control points, we set

$$b_0 = (0, h), \quad b_2 = (x_1, y_1), \quad b_4 = (l, 0)$$

for height h and length l of the body and (x_1, y_1) is a given point which represents also a grid point for the numerical solution of the problem. Furthermore, we want to guarantee a smooth connection to the other quadrants. This means that in b_4 we want to have slope infinity and in b_0 slope 0. Having information about the slope $m < 0$ in the point (x_1, y_1) we can define two additional control points b_1, b_3 as follows:

$$b_1 = ((h + m x_1 - y_1)/m, h), \quad b_3 = (l, ml + y_1 - m x_1)$$

ensuring the demanded differentiability properties. In this context we usually choose $m = -1.0$. Furthermore, the parameters l and h have to be chosen such that $b_{1,x} > 0$ and $b_{3,y} > 0$. To guarantee that the spline is C^1 on $[t_0, t_2]$ we set t_1 according to

$$t_1 = \frac{\|b_2 - b_1\|}{\|b_3 - b_2\| + \|b_2 - b_1\|},$$

where $\|.\|$ is the Euclidean norm. In Fig. 1 we show the construction in the first quadrant as well as the complete object.

In the optimization process using quadratic spline approximations the shape will be varied using different height and length parameters. Possible configurations for various length parameters can be seen in Fig. 2. In the optimization problem bounds on r and h have to be set to ensure physically sensible solutions.

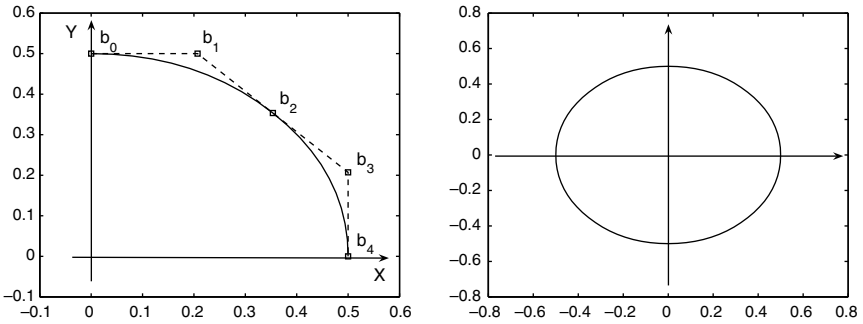

Fig. 1. Spline construction in first quadrant (left) and complete object (right).

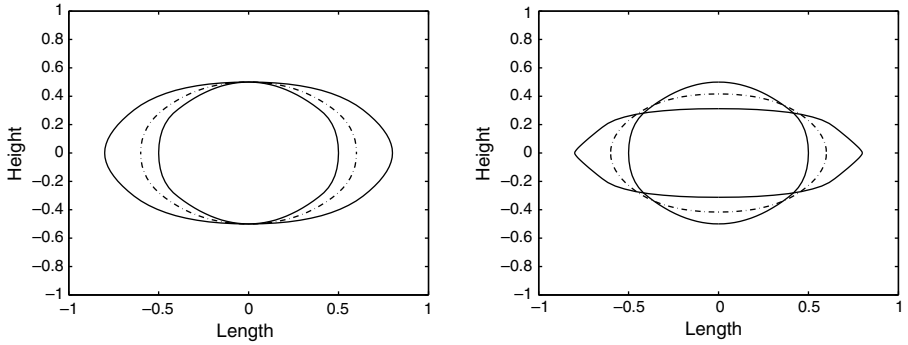

Fig. 2. Different shapes with constant height (left) and constant volume (right).

3.2. Approximation by cubic spline functions

To increase the space of admissible domains we also consider a description of the shape by cubic splines. The construction idea is the same as above. In this case the Bézier curve is defined by

$$b(t) = \sum_{j=0}^{3} b_j B_j^{(3)}(t).$$

For the composition we have for $i = 0, 1$

$$b(t) = \sum_{j=0}^{3} b_{3i+j} B_j^3\left(\frac{t - t_i}{t_{i+1} - t_i}\right) \quad \text{on} \quad t \in [t_i, t_{i+1}].$$

As control points for the composition of two cubic Bézier curves in the first quadrant we take in this case

$$b_0 = (0, h), \quad b_3 = (x_1, y_1), \quad b_6 = (l, 0)$$

and further

$$b_1 = (l/6, h), \quad b_5 = (l, h/6)$$

to guarantee differentiability at b_0 and b_6. For a smooth connection at b_3 we further set

$$b_2 = (x_1 - l/6, y_1 - mh/6), \quad b_4 = (x_1 + l/6, y_1 + mh/6)$$

with given slope $(1 \cdot l, m \cdot h)$ at b_3, where $m \in [0, -1]$. In this context we set $t_0 = 0$, $t_1 = 1/2$ and $t_2 = 1$. The grid point b_3 is not fixed and depends on the choice of coefficients c_l and c_h,

$$b_3 = (x_1, y_1) = (c_l \cdot l, c_h \cdot h).$$

To avoid conflict with the other control points, we have heuristic constraints on the choice of coefficients. In our calculations we set

$$0.5 < c_l < 0.8.$$

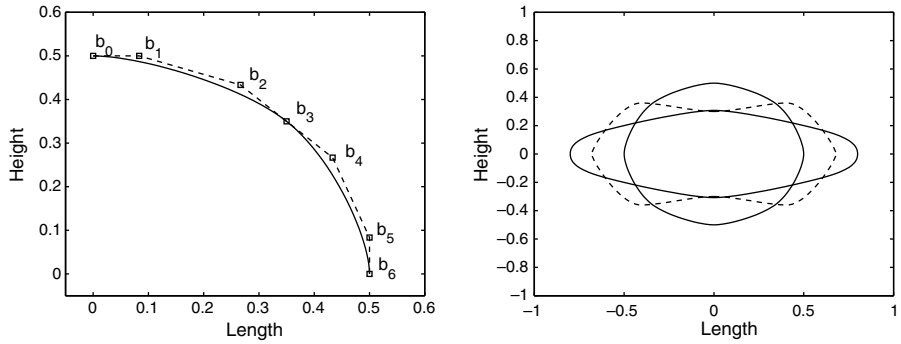

Fig. 3. Construction in the case of cubic spline approximation (left) and different shapes with constant volume (right).

For the choice of c_h we have more flexibility since shapes with $c_h > 1$ are also feasible. We set, e.g.

$$0.5 < c_h < 1.1.$$

Different shapes are shown in Fig. 3. Now it is also possible to consider a design with zero slope at the grid point b_3 as indicated by the dotted line. The modification of c_l and c_h leads to an adaptation of the mesh in each iteration step.

It turns out in Section 5 that it will also be important to consider a volume constraint. The volume Q is approximated by the area under the control polygon on the interval $[0, l]$. It yields in good approximation the volume of the described object.

$$Q = \sum_{i=1}^{6} (b_{i,x} - b_{i-1,x})(b_{i-1,y} + b_{i,y})/2 = \left(\left(\frac{5}{12} - \frac{m}{6}\right)x_1 + \left(\frac{5}{72} + \frac{7m}{72}\right)l\right)h + \frac{7}{12}y_1 l = \left(\left(\frac{5}{12} - \frac{m}{6}\right)c_l + \left(\frac{5}{72} + \frac{7m}{72}\right) + \frac{7}{12}c_h\right)lh.$$

4. Discretization and solution process

In this section our goal is to describe the overall numerical solution process. In that context we follow a discretize-then-optimize approach. The proposed scheme relies on the SQP method which in our framework involves the solution of an eigenvalue problem for the hydrodynamic stability. Both for the Navier–Stokes equations and for the associated eigenvalue problem the discretization is based on the finite element method. The efficient solution of the eigenvalue problem is a cornerstone of the presented optimization solver.

4.1. Solution of hydrodynamic and eigenvalue problem

The starting point to solve (1) is a variational formulation of the Navier–Stokes problem. With the notation $L := L^2(\Omega_q)$, $\widehat{H} := H^1(\Omega_q)^d$, and $H := \{v \in H^1(\Omega_q)^d, v_{|\Gamma_{\text{in}} \cup \Gamma_{\text{rigid}}} = 0\}$, let

$$\widehat{V} := \widehat{H} \times L, \quad V := H \times L \subset \widehat{V}.$$

For pairs $u = \{v,p\}$ and $\phi = \{\phi^v, \phi^p\} \in \widehat{V}$, we define the semilinear form

$$a(u;\phi) := \nu(\nabla v, \nabla \phi^v) + (v \cdot \nabla v, \phi^v) - (p, \nabla \cdot \phi^v) + (\phi^p, \nabla \cdot v),$$

and the right-hand side $f(\phi) := (f, \phi^v)$. Then, with a solenoidal extension $\hat{v}^{\text{in}} \in \widehat{V}$ of the inflow data v^{in}, we consider a solution $\hat{u} = \{\hat{v}, \hat{p}\} \in V + \{\hat{v}^{\text{in}}, 0\}$ of the problem

$$a(\hat{u};\phi) = f(\phi) \quad \forall \phi \in V. \tag{6}$$

We assume that the reference solution $\hat{u}$ is (locally) unique, that is, the Fréchet derivative $a'(\hat{u};\cdot,\cdot)$ is coercive. The variational formulation of the corresponding eigenvalue problem uses the derivative form

$$a'(\hat{u};\psi,\phi) := \nu(\nabla \psi^v, \nabla \phi^v) + (\hat{v} \cdot \nabla \psi^v, \phi^v) + (\psi^v \cdot \nabla \hat{v}, \phi^v) - (\psi^p, \nabla \cdot \phi^v) + (\phi^p, \nabla \cdot \psi^v),$$

and the bilinear form

$$m(\psi,\phi) := (\psi^v, \phi^v),$$

for arguments $\psi = \{\psi^v, \psi^p\}$ and $\phi = \{\phi^v, \phi^p\} \in V$. Then, the eigenvalue problem associated to the solution $\hat{u}$ determines $u = \{v,p\} \in V \backslash \{0\}$ by

$$a'(\hat{u};u,\phi) = \lambda m(u,\phi) \quad \forall \phi \in V. \tag{7}$$

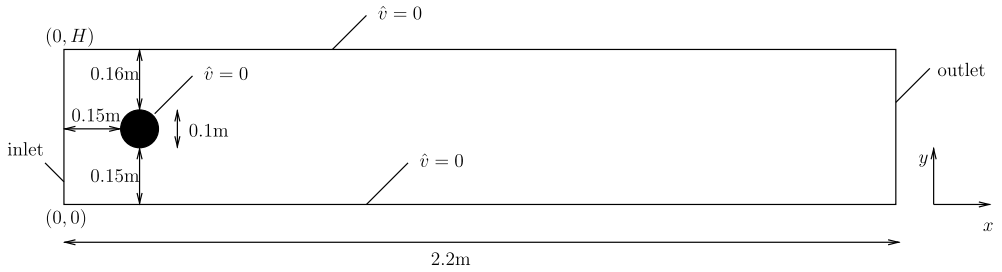

Fig. 4. Geometry of 2D benchmark configuration.

The 'primal' eigenfunctions are usually normalized by $m(u, u) = \|v\|^2 = 1$. For the following discussion, we assume that the eigenvalue of interest λ has *geometrical multiplicity one*. The case of higher geometrical multiplicity requires some obvious changes. Associated to the primal eigenfunction u, there is a 'dual' eigenfunction $u^* = \{v^*, p^*\} \in V\backslash\{0\}$ corresponding to λ that is determined by the 'dual' eigenvalue problem

$$a'(\hat{u}; \phi, u^*) = \lambda m(\phi, u^*) \quad \forall \phi \in V. \tag{8}$$

In order to solve (6)–(8) numerically by a Galerkin finite element method, the infinite dimensional spaces H and L are replaced by finite dimensional finite-element-spaces of functions which are piecewise mapped polynomials on a triangulation $\mathscr{T}_h$. The considered meshes are supposed to be *shape regular* and geometrically conforming (see [17]). They consist of curvilinear quadrilateral (or hexahedral) elements $\{K\}$ covering the domain $\bar{\Omega}_q$. For simplicity, we consider only *affine* meshes where each $K \in \mathscr{T}_h$ is affine equivalent to the reference element $\widehat{K} := (0, 1)^d$, i.e. $K = F_K(\widehat{K})$ with F_K affine and orientation preserving. The considered trial and test spaces $X_h \subset X$ consist of continuous, piecewise polynomial vector functions (so-called Q_k elements) for all unknowns,

$$X_h^{2,1} := \{(p_h, v_h) \in C(\bar{\Omega}_q)^{1+d} / p_h|_K \circ F_K \in Q_1(\widehat{K}); v_h|_K \circ F_K \in Q_2(\widehat{K})\}. \tag{9}$$

Here, $Q_r(\widehat{K}), r = 1, 2$, is the space of tensor-product polynomials of degree r on the reference element $\widehat{K}$, i.e.

$$Q_r(\widehat{K}) := \mathrm{span}\{x^i y^j z^k : 0 \leqslant i, j, k \leqslant r\}, \tag{10}$$

where $k = 0$ when $d = 2$.

The corresponding finite element subspaces are denoted by

$$L_h \subset L, \widehat{H}_h \subset \widehat{H}, H_h \subset H, \qquad \widehat{V}_h := L_h \times \widehat{H}_h, V_h := L_h \times H_h,$$

and $\hat{v}_h^{\mathrm{in}} \in \widehat{H}_h$ is a suitable interpolation of the boundary function $\hat{v}^{\mathrm{in}}$. Then, the discrete Navier–Stokes problem determines $\hat{u}_h := \{\hat{v}_h, \hat{p}_h\} \in V_h + \{\hat{v}_h^{\mathrm{in}}, 0\}$ by

$$a(\hat{u}_h; \phi_h) = f(\phi_h) \quad \forall \phi_h \in V_h. \tag{11}$$

The associated discrete primal and dual eigenvalue problems seek $u_h = \{v_h, p_h\}$ and $u_h^* = \{v_h^*, p_h^*\}$ in $V\backslash\{0\}$ and $\lambda_h \in \mathbb{C}$, such that

$$a'(\hat{u}_h; u_h, \phi_h) = \lambda_h m(u_h, \phi_h) \quad \forall \phi_h \in V_h, \tag{12}$$

$$a'(\hat{u}_h; \phi_h, u_h^*) = \lambda_h m(\phi_h, u_h^*) \quad \forall \phi_h \in V_h, \tag{13}$$

The eigenfunctions are usually normalized by $m(u_h, u_h) = m(u_h, u_h^*) = 1$. Eq. (6) has *saddle-point* structure due to the specific coupling of the pressure and the velocity. Therefore, the discretization must fulfill the so-called Babŭska-Brezzi (BB) condition which particularly guarantees a stable approximation of the pressure and avoids the occurrence of spurious pressure modes (see, e.g. [18]). One important advantage related to the choice of $X_h^{2,1}$ for the discretization is that this condition is automatically fulfilled and does not necessitate any additional stabilization terms (see, e.g. [18]).

The resulting nonlinear algebraic system of the hydrodynamic problem (1) is solved implicitly in a fully coupled manner by means of a damped Newton method. The involved Jacobian is directly derived from the analytical derivative of the variational system. The occurring linear subproblems are solved by the *generalized minimal residual method (GMRES)* preconditioned by means of multigrid iteration. Two specific features characterize the scheme: varying orders of the FEM ansatz on the mesh hierarchy and Vanka-type smoothers adapted to higher order discretization. We refer to [19] for more details.

The solution of the eigenvalue problem is a highly tedious task since the appearing problems are non self-adjoint. The considered approach for the eigenvalue computation uses a scheme which couples the Jacobi–Davidson method ([20,21]) with a multigrid process (for more details see [14,22]). This method shows to be highly efficient as compared to standard algebraic techniques. The overall solution process is implemented as part of the HiFlow project [23].

The advantages connected with this combined approach are mainly twofold. On the one hand, it allows in the context of nested iteration a better control of the best available eigenpair approximate at a given level. Especially, as opposed to the pure multigrid approach, eigenmodes which do not exist on the coarse levels can be nevertheless recovered on finer grids.

On the other hand, the ability to change the size of the projection space for the Rayleigh matrix allows to adaptively balance the multigrid and algebraic components. Algorithm 1 sketches the Jacobi–Davidson method combined with the multigrid scheme. The maximal basis size is denoted by n_B. The starting block vectors for the right (resp. left) eigenvectors are denoted by V_1 (resp. W_1). The matrices A and M in the Algorithm 1 correspond to the stiffness and mass matrix in Eq. (12).

Algorithm 1. (MJD(n_B, W_1, V_1)) for $k = 1$ to $k_{\max}$: do

- Step 1. Compute Rayleigh matrix: $H_k := W_k^H M V_k$.
- Step 2. Compute the smallest left/right eigenpair $\{\lambda_k, y_k, y_k^*\}$ of H_k.
- Step 3. Compute left/right Ritz vectors $x_k := V_k y_k$ and $x_k^* := W_k y_k^*$.
- Step 4. Compute residuals $r_k := (\lambda_k M - A)x_k$ and $r_k^* := (\bar{\lambda}_k M - A)x_k^*$.
- Step 5. If convergence exit.
- Step 6. Multigrid step $MG(t_k, r_k)$ and $MG^*(t_k^*, r_k^*)$. If $\dim(V_k) < n_B$ then set $W_{k+1} := [W_k, t_k^*]$ and $V_{k+1} := [V_k, t_k]$ else set $W_{k+1} := [x_k^*, t_k^*]$ and $V_{k+1} := [x_k, t_k]$.
- Step 7. Biorthogonalize (W_{k+1}, V_{k+1}).

Furthermore, a posteriori estimates in terms of the cell residuals accomplish simultaneous control of the error in the linearization and the error in the resulting eigenvalues. From these error estimates cell-wise error indicators are obtained that can guide the mesh refinement process [24,25].

4.2. Solution of optimization problem

To solve the optimization problems (4) and (5) an active-set SQP method is considered using a BFGS update (see, e.g. [26]). In each iteration step a quadratic subproblem is constructed and its solution yields a new iterate. The SQP approach can be interpreted as a Newton's method applied to the KKT optimality conditions of this quadratic subproblem. The inequality constraints are treated using an active-set strategy. In that framework an inequality constraint appears in the Lagrange formulation as an equality constraint if the bound is reached at the current design point and neglected otherwise. Hence in each iteration step only subproblems with equality constraints are solved. Here we want to sketch the algorithm for the example of an active stability constraint. We define the Lagrange function for (4) as follows

$$\mathscr{L}(q, \mu) = J(q) - \mu Re\{\lambda_{\min}(A(S(q)))\}.$$

To simplify notation we denote

$$Re(\lambda_{\min}(q)) := Re\{\lambda_{\min}(A(S(q)))\}.$$

The KKT conditions are given by

$$\frac{\partial \mathscr{L}(q,\mu)}{\partial q} = 0, \quad \frac{\partial \mathscr{L}(q,\mu)}{\partial \mu} = 0$$

resulting in

$$\begin{pmatrix} \nabla J(q) - \mu \nabla Re(\lambda_{\min}(q)) \\ Re(\lambda_{\min}(q)) \end{pmatrix} = \begin{pmatrix} 0 \\ 0 \end{pmatrix}.$$

The Jacobian of this system is given by

$$\mathscr{J}(q,\mu) = \begin{pmatrix} \nabla^2_{qq} \mathscr{L}(q,\mu) & -\nabla_q Re(\lambda_{\min}(q))^{\mathrm{T}} \\ \nabla_q Re(\lambda_{\min}(q)) & 0 \end{pmatrix}$$

such that a Newton iteration yields in our case the following quadratic subproblem in iteration step k

$$\begin{pmatrix} B^{(k)}(q^{(k)}) & -\nabla_q Re(\lambda^{(k)}_{\min}(q^{(k)}))^{\mathrm{T}} \\ \nabla_q Re(\lambda^{(k)}_{\min}(q^{(k)})) & 0 \end{pmatrix} \begin{pmatrix} p^{(k)} \\ \mu^{(k+1)} \end{pmatrix} = \begin{pmatrix} -\nabla_q J^{(k)}(q^{(k)}) \\ -Re(\lambda^{(k)}_{\min}(q^{(k)})) \end{pmatrix},$$

where $B^{(k)}(q^{(k)})$ represents an adequate approximation of the Hessian of the Lagrangian $\nabla^2_{qq}\mathscr{L}^{(k)}$. In our case this approximation is determined by the BFGS formula. The derivatives of the drag and the eigenvalue function with respect to the design variables are calculated by finite differences. This requires an additional function evaluation for each design variable. For the design variable vector we have the update

$$q^{(k+1)} = q^{(k)} + \tau^{(k)} p^{(k)},$$

where the parameter $\tau^{(k)}$ can be chosen by means of a line search method to ensure the feasibility of the newly computed solution. This may require many additional function evaluations. In practice the step size is determined heuristically to guarantee that the iterates stay within the feasible domain.

Remark. In order to obtain a feasible solution in case of violation of the inequality constraints the original optimization problem can be regularized in the following way:

$$\begin{aligned} &\min_q F_D(q) + \alpha\sigma \\ &\text{s.t.} \\ &Re(\lambda_{\min}(A(S(q)) + \sigma I) \geqslant 0, \\ &\underline{q} \leqslant q \leqslant \bar{q}, \end{aligned} \tag{14}$$

where σ plays the role of a shift coefficient with respect to the spectrum of $A(S(q))$ and α describes the regularization parameter. For the considered numerical experiments in Section 5 it turns out that this regularization is not needed.

Remark. The proposed SQP method relies on the differentiability of objective and constraint functions. For the computation of the Jacobian $\mathscr{J}$ the differentiability of the function of the smallest eigenvalue is needed for the computation of $\nabla Re(\lambda_{\min}(q))$. It has to be noted that this assumption may not be fulfilled in the case of eigenvalues with multiplicity larger than one (see [27] for details). During our calculations the authors did not encounter any problems related to this issue. In order to tackle this kind of problem the proposed scheme should be generalized towards derivative-free or non-smooth optimization algorithms.

Finally, we want to summarize the complete algorithm.

Algorithm 2.

- Step 1. Introduce suitable function approximation for the geometry and determine initial design variables $q^{(0)} = (q_1, \ldots, q_n)$, set $k{:=}0$.
- Step 2. Create mesh depending on design variable vector $q^{(k)}$.
- Step 3. Solve flow problem to obtain drag force $F_D(q^{(k)})$.
- Step 4. Solve eigenvalue problem to obtain $Re(\lambda_{\min}(q^{(k)}))$.
- Step 5. Determine derivatives of $F_D(q^{(k)})$ and $Re(\lambda_{\min}(q^{(k)}))$ with respect to design variables by finite differences.
- Step 6. Solve KKT system of the SQP algorithm to obtain direction $p^{(k)}$.
- Step 7. Determine suitable step length $\tau^{(k)}$.
- Step 8. Update design variable vector $q^{(k+1)} = q^{(k)} + \tau^{(k)} p^{(k)}$.
- Step 9. If termination criterion is reached then STOP else set $k{:=}k + 1$ and goto Step 2.

Remark. In the previously derived algorithm the major computational costs are related to steps 4 and 5, especially for the computation of the eigenvalues of the linearized Navier–Stokes operator. In step 5 the derivatives with respect to the different design variables can be computed independently. For a large number of parameters this step can obviously be fulfilled on a parallel machine where each process computes the derivative of one of the design variables.

5. Numerical examples

5.1. Configuration setup

We consider the benchmark channel flow around a certain body in two dimensions as described in [12]. In the initial configuration the body is assumed to be a cylinder. Here we want to pursue the approach to find the optimal shape of the body which minimizes the drag force and guarantees hydrodynamic stability.

The geometry of the channel is depicted in Fig. 4.

In the two dimensional case for the considered benchmark, the channel is 2.2 m in length and $H = 0.41$ m in width. The center of the cylinder is located at (0.2 m, 0.2 m) with a diameter of $D = 0.1$ m such that the configuration is not totally symmetric. The velocity at the inlet is prescribed by

$$\hat{v}_1(0,y) = 4|V_m|\frac{y(H-y)}{H^2}, \quad \hat{v}_2(0,y) = 0,$$

where $|V_m|$ denotes the maximum norm of the velocity at the inlet. The Reynolds number is defined by

$$Re = \frac{\overline{V}D}{\nu}, \quad \overline{V} = 2/3|V_m|,$$

then yielding to a Reynolds number of around 20 for $\nu = 10^{-3}$.

5.2. Parameter studies based on forward simulation

The goal of this section is to determine for which parameters the effect of a transition from unstable to stable behaviour can be observed. This section has to be understood as a preliminary step in order to define an adequate problem setup for the shape optimization process considered in our context.

In particular we have to determine the critical Reynolds number leading to unstable flow. It is closely related to the inflow velocity V_m. If the inlet velocity is too low one always has a stable regime and an unstable one if the velocity is too high. Calculations show that for the benchmark configuration (I) the bifurcation point occurs at around $V_m = 0.19$ m/s. An overview of the obtained bifurcation points for configurations with different length l and height h of the considered body is shown in Table 1.

One clearly observes that for long and flat designs (II, III) the bifurcation point occurs at a larger velocity than for short and steep designs (IV, V).

To get an insight of the drag and stability behaviour for the whole feasible domain we first determine these values for various configurations of l and h for fixed inflow velocity $V_m = 0.19$ m/s. The corresponding results are shown in Figs. 5 and 6.

Table 1
Inflow velocities at which bifurcation point occurs for different configurations

Configuration	Velocity V_m (m/s) at bifurcation point
(I) $l = 0.05$ m, $h = 0.05$ m	0.1896
(II) $l = 0.08$ m, $h = 0.05$ m	0.1963
(III) $l = 0.08$ m, $h = 0.03$ m	0.2222
(IV) $l = 0.03$ m, $h = 0.05$ m	0.1830
(V) $l = 0.03$ m, $h = 0.08$ m	0.1530

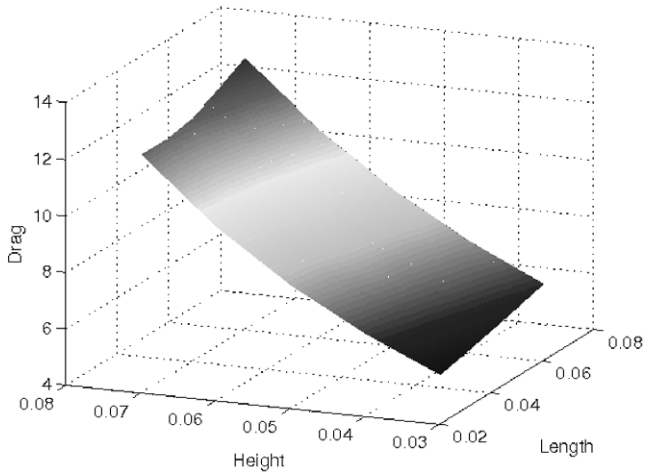

Fig. 5. Drag force acting on the body assuming different length and height.

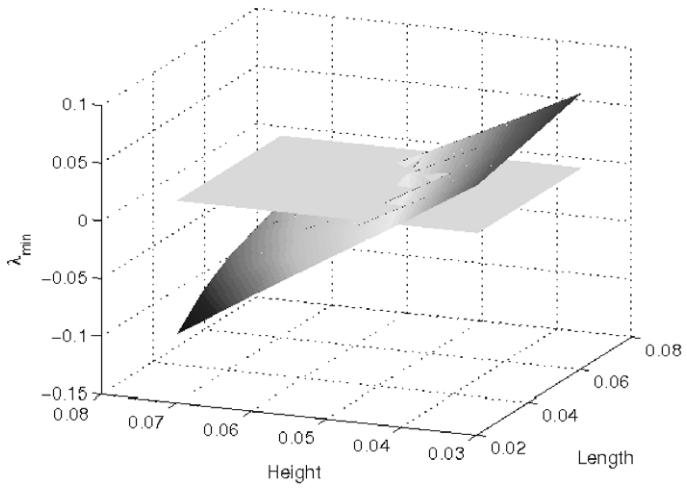

Fig. 6. Smallest eigenvalues of the linearized Navier–Stokes operator assuming different length and height of the body.

For constant h we observe an increase of the drag force for increasing l. The same holds vice versa for constant l. The smallest value occurs for the smallest values of l and h. Comparing the magnitudes of the change we notice that the influence of h is much larger as shown in Table 2. Therefore, the variation of h is more crucial with respect to the drag behaviour.

Concerning the stability behaviour we notice a tendency towards instability for increasing h. For increasing l, however, we have a slight increase towards stability. This corresponds to the intuition that long and flat objects yield indeed stability. Again, the influence of h is here larger than that of l. The corresponding results are summarized in Table 3.

5.3. Shape optimization assuming quadratic spline approximation

We first consider the optimization problem (4) and initially assume that the height h of the body is fixed at $h = 0.05$ m and the length l is taken as design variable. This implies that we first allow volume and surface changes of the bodies. Lower and upper bounds are set on the length parameter l to avoid physically infeasible solutions.

$$\min_l J(l) = F_D(l)$$
$$\text{s.t.}$$
$$Re(\lambda_{\min}(l)) \geqslant 0,$$
$$0.03\ \text{m} \leqslant l \leqslant 0.08\ \text{m}.$$

Our starting point is the benchmark configuration (cf. Fig. 7) and we choose an inflow velocity $V_m = 0.195$ m/s for which we have an unstable behaviour indicated by the negative real part of the smallest eigenvalue, $Re(\lambda_{\min}) = -0.02036$. The value of the drag force in this case is $F_D = 6.986$ N.

Our optimization with respect to the length parameter l and fixed height h yields the optimized design shown in Fig. 8. The obtained optimal length is $l = 0.0785$ m. Furthermore, we have $F_D = 7.791$. Contrary to our goal to minimize the drag we recognize that the drag force is higher than for the initial design. This increase, however, is necessary to avoid a violation of the stability constraint which is now active, $Re(\lambda_{\min}) = 5.7 \cdot 10^{-6}$.

In a next step we consider the height h as additional design variable. In this case we obtain an optimum at the lower bound of the box constraints for both parameters, $l = h = 0.03$ m. For the given inflow velocity this design is stable and the

Table 2
Drag force for different configurations

Drag force F_D	$h = 0.035$ m	$h = 0.045$ m	$h = 0.055$ m	$h = 0.065$ m
$l = 0.035$ m	4.955	6.179	7.664	9.481
$l = 0.045$ m	5.141	6.360	7.832	9.622
$l = 0.055$ m	5.343	6.575	8.058	9.856
$l = 0.065$ m	5.560	6.816	8.329	10.154
$l = 0.075$ m	5.793	7.082	8.638	10.522

Table 3
Real part of smallest eigenvalue of linearized Navier–Stokes operator for different configurations

$Re(\lambda_{\min})$	$h = 0.035$ m	$h = 0.045$ m	$h = 0.055$ m	$h = 0.065$ m
$l = 0.035$ m	0.0387	−0.0007	−0.0373	−0.0728
$l = 0.045$ m	0.0444	0.0075	−0.0267	−0.0596
$l = 0.055$ m	0.0503	0.0150	−0.0178	−0.0493
$l = 0.065$ m	0.0564	0.0220	−0.0098	−0.0403
$l = 0.075$ m	0.0628	0.0289	−0.0023	−0.0324

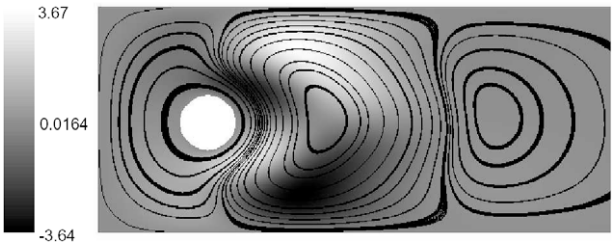

Fig. 7. Streamlines of eigenfunction associated to the smallest eigenvalue for the initial design, i.e. $l = 0.05$ m, $h = 0.05$ m, $V_m = 0.195$ m/s. This configuration leads to $Re(\lambda_{\min}) = -0.02036$ and $F_D = 6.986$. The function plot corresponds to the first component of the eigenfunction.

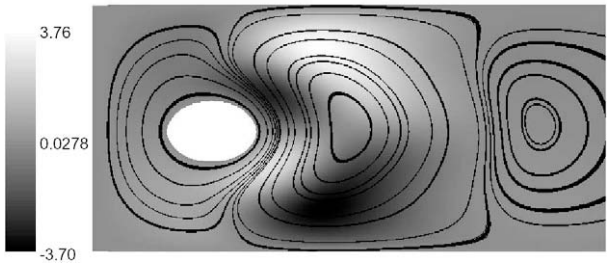

Fig. 8. Streamlines of eigenfunction associated to the smallest eigenvalue for the optimal solution assuming fixed height $h = 0.05$ m and $V_m = 0.195$ m/s. This setting leads to $l = 0.0785$ m, $F_D = 7.791$ and $Re(\lambda_{min}) = 5.7 \cdot 10^{-6}$. The function plot corresponds to the first component of the eigenfunction.

drag reaches its smallest possible value, as is also obvious from Figs. 5 and 6. It is not surprising that in this situation the optimal solution leads to the smallest possible volume of the body. In order to avoid this effect we assume a fixed volume of the body in all further calculations.

Therefore, we repeat our parameter study with variable length l. In the case of the quadratic spline approximation we use the volume of an ellipsoid, given by $Q = \pi lh$, to approximate the volume of the body. In this case we observe (cf. Fig. 9) a monotone decrease of the drag force with increasing l and an increase of the real part of the smallest eigenvalue which is equivalent to a tendency towards a stability of the system.

A summary of this result is plotted in Fig. 10 which shows the dependence of the length and the inflow velocity at which the bifurcation occurs. We observe a monotone increase for longer and flatter objects.

Concerning the optimization problem we extend the original formulation (4) by an additional constraint on the volume of the body. We only want to accept designs which leave the volume of the body constant and its value is taken for the benchmark configuration

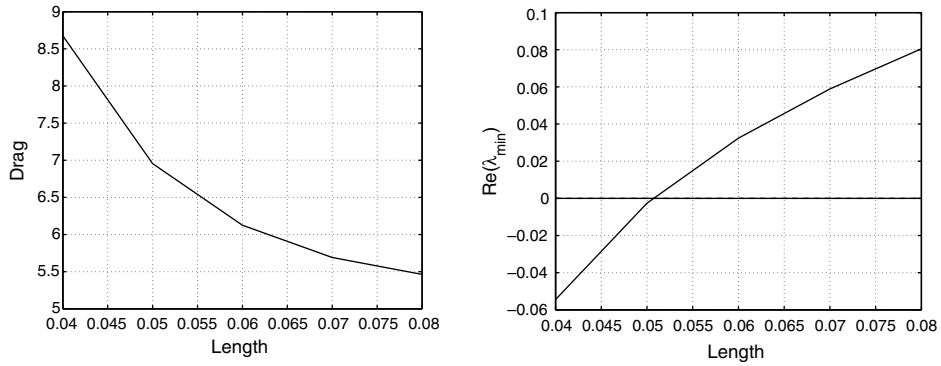

Fig. 9. Drag force (left) and stability (right) behaviour for shape variations assuming fixed volume and inflow velocity $V_m = 0.19$ m/s.

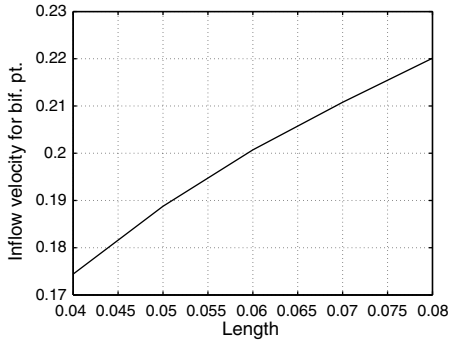

Fig. 10. Inflow velocity at which bifurcation point occurs in dependence of length.

$$\min_l J(l, h(l)) = F_D(l, h(l))$$
s.t.
$$Re(\lambda_{\min}(l, h(l))) \geqslant 0,$$
$$\mathrm{Vol}(\Omega_q) = \mathrm{const},$$
$$0.03\ \mathrm{m} \leqslant l \leqslant 0.08\ \mathrm{m},$$
$$0.03\ \mathrm{m} \leqslant h \leqslant 0.08\ \mathrm{m}.$$

The optimization program yields $J = 5.388$ and $\lambda_{\min} = 0.0675$ with $l = 0.08$ m and $h = 0.0312$ m. The drag force is in this case reduced by 22.9% compared with the initial setting. Moreover, we obtain clearly a stable regime since the real part of the smallest eigenvalue is strictly positive. The optimized design and the first component of the eigenfunction can be seen in Fig. 11.

Remark. It is important to notice that a change from unstable behaviour to stable behaviour can be achieved by modifying alone the design of the object while leaving all other parameters constant.

5.4. Shape optimization assuming cubic spline approximation

Using a cubic spline description of the body as presented in Section 3.2, the design space is enlarged as compared to the setup in Section 5.3. We therefore expect a further decrease of the objective function. In this context, we consider five design variables which are the length of the body l, its height h, the coefficients for the position of the grid point c_l and c_h and the slope m in the grid point (see Section 3 for further details). This leads to the design variable vector

$$q = (l, h, m, c_l, c_h).$$

We solve optimization problem (5) with corresponding volume constraint. We consider an initial design similar to the setup corresponding to Fig. 7, which is represented in this case by $q^{(0)} = (0.05, 0.05, -1.0, 0.7, 0.7)$. As in Section 5.2 this configuration leads to an unstable solution for the inflow velocity $V_m = 0.195$ m/s. The optimal solution obtained by means of the proposed method is found to be

$$l = 0.08\ \mathrm{m}, \quad h = 0.03\ \mathrm{m}, \quad m = -1.0, \quad c_l = 0.8, \quad c_h = 0.656.$$

As compared to the case of quadratic spline approximation we observe a slight reduction of the drag force in this situation, since $J = 5.361$ instead of $J = 5.388$. The optimized design is also more stable with the real part of the smallest eigenvalue being $Re(\lambda_{\min}) = 0.07793$ instead of $Re(\lambda_{\min}) = 0.0675$. However, it has to be noted that the volume restriction differs for

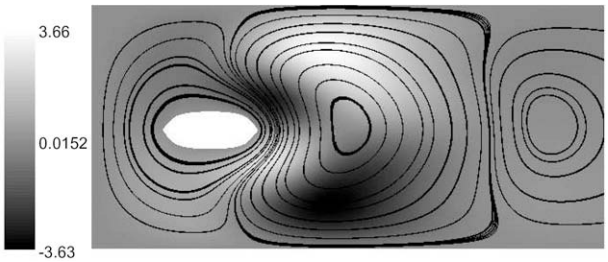

Fig. 11. Streamlines of the eigenfunction associated to the smallest eigenvalue for the optimal solution assuming fixed volume and $V_m = 0.195$ m/s. This setting leads to $l = 0.08$ m, $h = 0.0312$ m, $F_D = 5.388$ and $Re(\lambda_{\min}) = 0.0675$. The function plot corresponds to the first component of the eigenfunction.

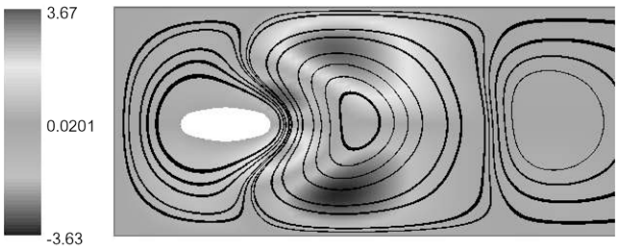

Fig. 12. Streamlines of eigenfunction of smallest eigenvalue for optimized configuration assuming fixed volume and $V_m = 0.195$ m/s. This setting leads to $q = (0.08, 0.03, -1.0, 0.8, 0.656)$, $F_D = 5.361$ and $Re(\lambda_{\min}) = 0.07793$. The function plot corresponds to the first component of the eigenfunction.

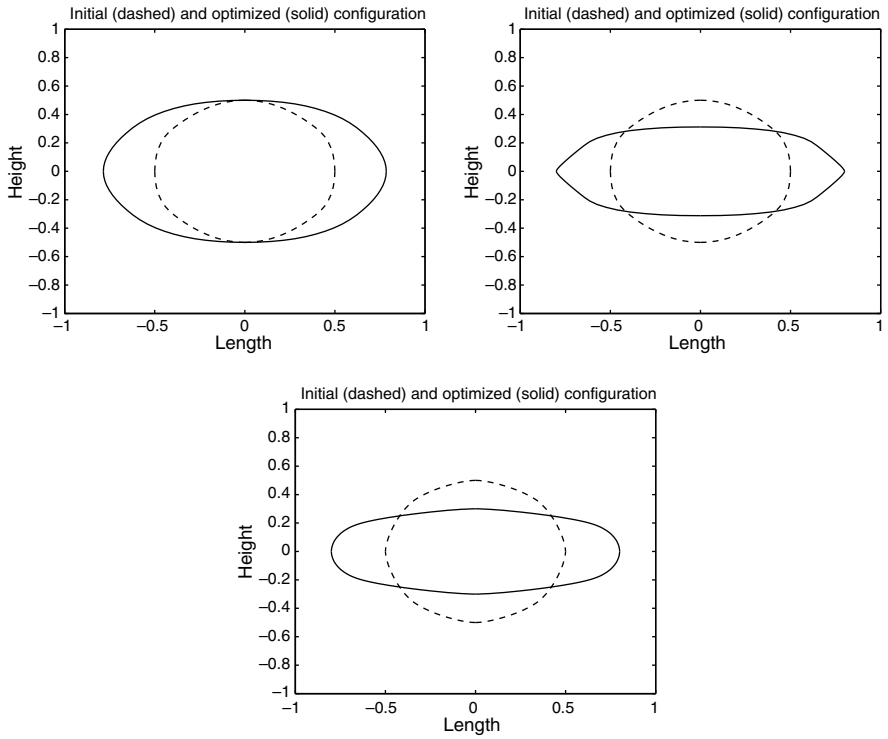

Fig. 13. Initial (dashed) and optimized (solid) configurations for the following settings. Quadratic spline approximation, fixed height (upper left); Quadratic spline approximation, fixed volume (upper right); cubic spline approximation, fixed volume (bottom).

the cubic spline approximations since we use an approximation by the area under the control polygon instead of an ellipsoid (see Section 3.2).

The eigenfunction associated to the smallest eigenvalue for the optimized configuration is shown in Fig. 12. Again we have achieved a transition from an unstable design to a stable design only by solving a shape optimization problem.

An overview depicting the different initial and optimized configurations is given in Fig. 13.

6. Conclusion

In this paper we propose a numerical method towards shape optimization for flow problems assuming constraints with respect to hydrodynamic stability. As an example we consider the flow around a body in a channel and use parameterizations of this body by quadratic and cubic spline functions. The goal is to minimize the drag force acting on the body by modifying its shape while ensuring hydrodynamic stability. The numerical simulations clearly validate the proposed approach and show that a transition of an unstable design into a stable one can be attained by solely changing the shape of the body keeping all other parameters constant. The resulting geometries lead to long and flat bodies which corresponds to common intuition. Moreover, our investigations clearly show that shape optimization can only partly contribute to the stability behaviour and that the boundary conditions, e.g. the inflow velocity, play also an important role in that context.

Since this work has a preliminary character several extension are possible. An important issue is to investigate other shape parameterizations, especially techniques leading to an increase of flexibility in the description of the geometry. Concerning the numerical solution of the problem the application of derivative-free and non-smooth algorithms is envisaged to deal with the possibly non-differentiable eigenvalue function. Finally, the highly CPU time demanding computations which are related to the solution of the underlying problem requires for complex configurations the use of techniques of high performance computing. In that context further developments towards 3D settings are the object of current research.

References

[1] D. Joseph, Stability of Fluid Motions, Springer-Verlag, 1976.
[2] P. Drazin, W. Reid, Hydrodynamic Stability, Cambridge University Press, 1982.
[3] G. Galdi, M. Padula, A new approach to energy theory in the stability of fluid motion, Arch. Rational Mech. Anal. 110 (3) (1990) 187–286.
[4] B. Straughan, The Energy Method, Stability and Nonlinear Convection, Springer, 1992.
[5] D. Sattinger, The mathematical problem of hydrodynamic stability, J. Math. Mech. 19 (1970) 797–817.
[6] S. Chandrasekhar, Hydrodynamic and Hydromagnetic Stability, Dover Publ., 1981.
[7] M. Delfour, J.-P. Zolésio, Shapes and Geometries: Analysis, Differential Calculus and Optimization, SIAM, 2001.

[8] M. Gunzburger, Perspectives in Flow Control and Optimization, SIAM, 2003.
[9] J. Haslinger, R. Mäkinen, Introduction to Shape Optimization: Theory, Approximation and Computation, SIAM, 2003.
[10] A. Henrot, J. Sokolowski, Mathematical challenges in shape optimization, Control and Cybernetics 34 (1) (2005) 37–57.
[11] B. Mohammadi, O. Pironneau, Applied Shape Optimization for Fluids, Oxford University Press, 2001.
[12] M. Schäfer, S. Turek, Benchmark computations of laminar flow over a cylinder, Notes in Numer. Fluid Mech. 52 (1996) 856–869.
[13] Y. Ding, M. Kawahara, Three-dimensional linear stability analysis of incompressible viscous flows using the finite element method, Int. J. Numer. Meth. Fluids (31) (1999) 451–479.
[14] V. Heuveline, Finite element approximations of eigenvalue problems for elliptic partial differential operators, Habilitationsschrift, Ruprecht-Karls-Universität Heidelberg, 2002.
[15] D. Bucur, A. Henrot, Minimization of the third eigenvalue of the Dirichlet Laplacian, Proc. Roy. Soc. London 456 (2000) 985–996.
[16] G. Farin, Curves and Surfaces for Computer Aided Geometric Design, Academic Press, Boston, 1988.
[17] P. Ciarlet, The Finite Element Method for Elliptic Problems, North-Holland, 1987.
[18] F. Brezzi, M. Fortin, Mixed and Hybrid Finite Element Methods, Springer-Verlag, 1991.
[19] V. Heuveline, On higher-order mixed FEM for low Mach number flows: application to a natural convection benchmark problem, Int. J. Numer. Math. Fluids 41 (12) (2003) 1339–1356.
[20] M. Sadkane, Block Arnoldi and Davidson methods for unsymmetric large eigenvalue problems, Numer. Math. 64 (1993) 195–211.
[21] G. Slejpen, H.A. van der Vorst, A Jacobi–Davidson iteration method for linear eigenvalue problems, SIAM Rev. 42 (2) (2000) 267–293.
[22] V. Heuveline, C. Bertsch, On multigrid methods for the eigenvalue computation of nonselfadjoint elliptic operators, East–West J. Numer. Math. 8 (2000) 275–297.
[23] V. Heuveline, HiFlow, a general purpose finite element toolbox. <http://www.hiflow.de>, 2000.
[24] V. Heuveline, R. Rannacher, Adaptive FEM for eigenvalue problems with application in hydrodynamic stability analysis, J. Numer. Math. (accepted for publication).
[25] C. Johnson, R. Rannacher, M. Boman, Numerics and hydrodynamic stability: toward error control in computational fluid dynamics, SIAM J. Numer. Anal. 32 (4) (1995) 1058–1079.
[26] J. Nocedal, S. Wright, Numerical Optimization, Springer-Verlag, 1999.
[27] T. Kato, Perturbation Theory for Linear Operators, Springer-Verlag, 1966.